专题：大陆俯冲带

评 述

俯冲隧道中的部分熔融和壳幔相互作用：实验岩石学制约

章军锋[①]*，王春光[②]，续海金[①]，王超[①]，许文良[②]

① 中国地质大学地质过程与矿产资源国家重点实验室, 武汉 430074;
② 吉林大学地球科学学院, 长春 130061
* E-mail: jfzhang@cug.edu.cn

摘要   俯冲隧道模型提出, 俯冲板片界面相互作用是实现地球表层与内部之间物质和能量交换的基本机制. 由于大陆岩石圈与大洋岩石圈在物质组成和状态上的显著差异, 其深部物理和化学过程及壳幔相互作用产物必然出现一系列差异. 许多实验岩石学研究已经为大洋俯冲隧道中可能发生的硅酸盐和碳酸盐岩石的部分熔融和壳幔相互作用提供了资料. 无论是基性还是中酸性硅酸盐岩体系, 取决于部分熔融发生的压力或深度, 熔体是具有或不具有埃达克岩性质的花岗质熔体. 微量 CO_2 即可大幅降低橄榄岩的熔点, 所形成的碳酸盐熔体可有效萃取岩石体系中不相容微量元素. 这些硅饱和或不饱和熔体均可以在俯冲隧道或地幔深部条件下与地幔楔橄榄岩发生反应, 形成复杂的反应过程和产物. 但已有的实验结果主要是针对大洋岛弧环境条件而不是大陆俯冲带的环境. 因此, 高温高压实验需要充分考虑大陆俯冲隧道中板片-地幔界面上各种不同成分地壳及其衍生的熔/流体成分与不同橄榄岩之间的反应, 并结合大陆俯冲带岩石部分熔融和壳幔相互作用的地质证据, 以阐明大陆俯冲隧道过程中的变质脱水、部分熔融和地幔交代等问题.

关键词
俯冲隧道
部分熔融
壳幔相互作用
高温高压实验

地壳与地幔之间的物质和能量的交换决定了地壳和地幔的演化、改造、构造-岩浆活动和大规模成矿作用. 传统板块构造学说认为, 大洋俯冲带是壳幔相互作用最为活跃的区域(例如, Allègre, 1982; Zindler和Hart, 1986; Tatsumi和Eggins, 1995). 在洋中脊形成的玄武岩和海底沉积物在俯冲过程中变质脱水, 并导致上覆地幔楔发生部分熔融作用(例如, Bebout, 2007; Spandler和Pirard, 2013), 形成大规模岛弧岩浆活动、成矿作用和产生新的大陆地壳(例如, Schmidt和Poli, 1998; Rudnick和Gao, 2003; Manning, 2004). 低密度玄武质洋壳俯冲过程中形成高密度的榴辉岩, 使冷的大洋岩石圈俯冲至地幔过渡带底部甚至核-幔边界, 形成大洋岩石圈的再循环, 构成地球上最宏伟的壳幔交换过程, 并深刻影响生命的起源和演化(例如, Bercovici和Karato, 2003). 近30年的研究成果表明, 相对于温度高和发育同俯冲部分熔

融作用的大洋俯冲带, 大陆俯冲带温度低、缺乏同俯冲脱水部分熔融作用, 但常见折返的超高压岩片(例如, Chopin, 2003; Liou等, 2009; Zheng, 2009)和同折返或碰撞后岩浆作用(例如, Zhao等, 2012), 也同样可以产生显著的壳幔相互作用(例如, Beaumont等, 2009; Guillot等, 2009; 赵子福和郑永飞, 2009; Zheng, 2012; Hermann和Rubatto, 2014). 由于洋壳和陆壳物质组成上的差异, 必然造成陆壳物质和洋壳物质与岩石圈地幔相互作用性质上的差异. 相应地, 由于大陆地壳物质组成与地幔物质组成的巨大差异, 大陆地壳的深俯冲和折返也必然会对上覆岩石圈或软流圈地幔性质和大陆板块汇聚边界的结构、组成、变形和演化进程造成巨大影响(Zheng, 2012; Yang D B等, 2012; Xu W L等, 2013). 这一过程在传统的板块构造学说中并未涉及. 对陆壳深俯冲和折返过程中不同类型深俯冲板片的部分熔融和熔体与地幔楔岩石相互作用的深入研究, 将是认识和发展大陆俯冲隧道模型的关键. 分析和总结大洋深俯冲过程中的部分熔融和壳幔相互作用, 可以为解析大陆俯冲带构造过程及其产物提供有益的启发和借鉴, 对进一步发展和完善板块构造理论具有重要的科学意义.

1　大陆俯冲隧道概念的提出

俯冲隧道指汇聚板块边缘下伏俯冲板片与上覆板片之间的空间及其中发生运动的物质, 是板块界面相互作用的产物. 汇聚板块之间的物理和化学作用可以出现在各种空间和时间尺度上, 对俯冲带过程非常关键. 认识俯冲带板块界面的性质, 是理解板块边缘相互作用的关键. 与板块构造理论一样, 为研究板块界面相互作用所提出的俯冲隧道概念, 起初也是建立在对大洋俯冲带构造认识的基础上(例如, Shreve和Cloos, 1986; Cloos和Shreve, 1988a, 1988b), 然后被拓展到大陆俯冲带(例如, Beaumont等, 2009; Guillot等, 2009; Zheng, 2012; 郑永飞等, 2013). 俯冲大洋岩石圈板片上的地壳物质(洋壳玄武岩和海底沉积物)受地幔楔隧道壁的机械刮削作用而拆离成不同大小的地壳碎块, 经历不同程度的变形和变质, 形成大洋俯冲隧道(Bebout, 2007; Spandler和Pirard, 2013)(图1(a)). 大洋俯冲隧道模型可以合理解释大洋俯冲带变质岩的产出(例如, Beaumount等, 1999; Gerya等, 2002; Guillot等, 2009).

郑永飞等(2013)提出, 大陆碰撞带俯冲隧道中不仅有俯冲大陆岩石圈上层在不同深度发生拆离而来的物质, 而且有从地幔楔底部被刮削下来的不同大小的地幔岩石碎块(图1(b)). 大陆俯冲带常常具有洋壳和陆壳复合性质, 超高压变质岩的原岩类型变化很大(Zheng, 2012), 例如在阿尔卑斯-喜马拉雅和天山-乌拉尔这类弧-陆碰撞造山带, 作为新生地壳的特提斯型玄武岩被俯冲到地幔深度经受超高压变质作用; 而在另一类陆-陆碰撞造山带, 例如大别-苏鲁和挪威西部片麻岩省中, 则是古老大陆基底和上覆沉积盖层被俯冲到地幔深度经受超高压变质作用. 卷入大陆俯冲隧道的地壳物质可能既有俯冲洋壳的玄武岩、辉长岩和大洋沉积物, 也有俯冲陆壳的基底花岗岩、麻粒岩以及沉积盖层(Dai等, 2015; Zhou等,
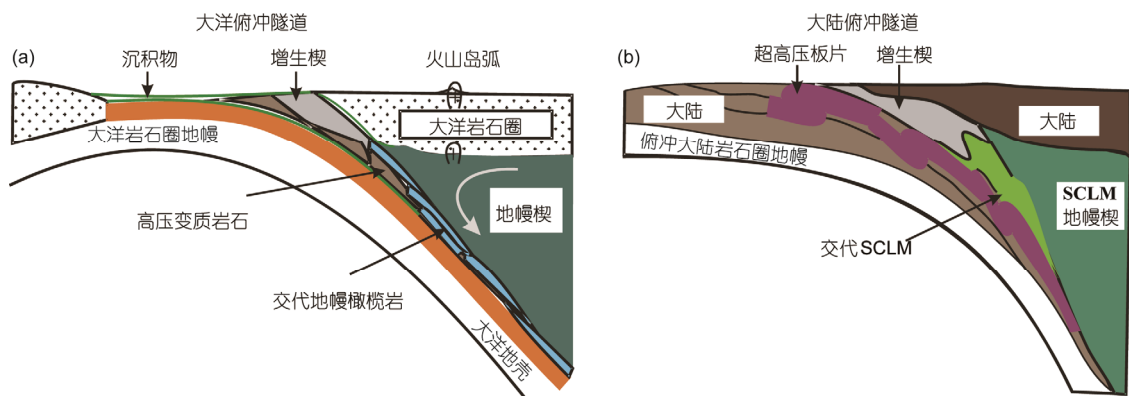

图 1　大洋和大陆俯冲隧道模型示意图

(a) 大洋俯冲隧道: 地幔楔温度高、黏度低、水活度高, 发育同俯冲脱水部分熔融作用, 薄(<1 km 至>10 km); (b) 大陆俯冲隧道: 地幔楔温度低、黏度高、水活度低, 发育同折返或碰撞后岩浆作用, 厚(>5 km 至>30 km). 据 Guillot 等(2009)和 Zheng(2012)

2015). 在大陆岩石圈俯冲至大陆岩石圈之下的阿尔卑斯型俯冲带中, 俯冲板片上覆的地幔楔既可以具有古老成因(克拉通贫瘠地幔), 也可以具有新生成因(弧下富化地幔). 这些不同来源的物质在大陆俯冲隧道内发生物理混合和化学反应, 经历不同程度的变质、变形乃至局部深熔作用, 形成不同型式的高压-超高压构造混杂岩. 与大洋俯冲隧道上覆地幔楔相比, 大陆俯冲带岩石圈地幔楔具有高黏滞度、低温度和低水活度等特点, 因而在俯冲过程中难以发生显著的脱水和熔融过程(例如, Liu等, 2006; Wu等, 2006; Xu H J等, 2013), 但是在变质峰期或折返早期, 俯冲地壳在俯冲隧道内的部分熔融作用比较普遍(例如, Wallis等, 2005; Liu等, 2010; Gao等, 2012; Guo等, 2012; Chen等, 2013a, 2013b; Xu H J等, 2013; Song等, 2014a; Wang等, 2014), 同样会引发显著的壳幔相互作用. 虽然大陆俯冲带超高压地体有大有小、折返速率有快有慢、深熔程度有高有低, 但是最新的一些研究表明大陆碰撞带的高压/超高压岩石的变质变形、深熔及壳幔相互作用的特征基本上也都可以根据大陆俯冲隧道过程予以解释(例如, Beaumont等, 1999; Guillot等, 2009; Zheng, 2012; 郑永飞等, 2013).

2 大陆俯冲隧道中的部分熔融作用

部分熔融会导致俯冲地壳的化学分异, 为碰撞和造山相关壳幔相互作用和岩浆活动提供物质来源, 而且对降低超高压岩石的流变强度而导致超高压地体的快速隆升有重要意义(例如, Labrousse等, 2011; Whitney等, 2009). 在过去近十年的研究中, 大陆俯冲带超高压变质岩中不同程度部分熔融的基本事实已经获得基本确认并受到了很多的关注(例如, Zheng等, 2011). 对包括大别造山带(例如, Guo等, 2012; Liu等, 2013; Liu P L等, 2014, 2015)和苏鲁造山带(例如, Wallis等, 2005; 刘福来等, 2009; Liu等, 2010, 2012; Zong等, 2010; Xu H J等, 2012b, 2013; Chen等, 2013a, 2013b, 2014; Song等, 2014a, 2014b; Wang等, 2014)、哈萨克斯坦Kokchetav地体(例如, Shatsky等, 1999)、德国Bohemian地体(例如, Massone, 2003)、挪威西片麻岩区(例如, Gordon等, 2013; Labrousse等, 2011)等典型超高压变质带混合岩的深入研究表明, 含水矿物(如多硅白云母和硬柱石等)在折返过程中的脱水分解及名义上无水矿物羟基出溶可能是导致超高压

变质地体发生部分熔融的关键(例如, Hermann, 2002; Patiño Douce, 2005; Auzanneau等, 2006; Hermann等, 2006; Zheng等 2011; Guo等, 2012; Gao等, 2012; Chen等, 2013a, 2013b; Liu Q等, 2013; Xu H J等, 2013). 超高压岩石的部分熔融作用是大陆俯冲带内深部流体活动的重要组成部分(例如, Zheng, 2012; Hermann等, 2013; Hermann和Rubatto, 2014). 在Kokchetav和Bohemian地体(例如, Shatsky等, 1999; Massone, 2003)的峰期变质温度较高, 足以导致超高压岩石的脱水部分熔融. 而对其他大多数相对低峰期变质温度的超高压地体来说, 发生部分熔融的条件包括等温或升温折返过程中的含水矿物分解(例如, Auzanneau等, 2006; Whitney等, 2009; Gao等, 2012, 2013; Liu等, 2013)和外来流体渗透(例如, Gordon等, 2013; Liu P L等, 2014).

超高压岩石中发生部分熔融的地质证据包括深熔作用形成的长英质脉体(图2(a)~(c))和薄片尺度的部分熔融显微地质结构(例如, 曾令森等, 2011; Wallis等, 2005; Zhao等, 2007; Xia等, 2008; Liu等, 2012; Gao等, 2012, 2013; Chen等, 2013a, 2013b; Xu H J等, 2013; Liu P L等, 2014; Wang等, 2014). 对混合岩的同位素年代学研究表明, 超高压岩石的部分熔融可以发生在折返早期的含柯石英超高压榴辉岩相(例如, Guo等, 2012; Chen等, 2013a, 2013b)、高压榴辉岩相(例如, Liu等, 2013; Xu H J等, 2013)和高压麻粒岩相(例如, Xu H J等, 2013)条件下. 超高压岩石中部分熔融的显微地质证据主要包括峰期矿物(如石榴石和单斜辉石)中的长英质多相固体包体(例如, Stöckhert等, 2001; Hwang等, 2003; Korsakov和Hermann, 2006; 曾令森等, 2009; Gao等, 2012; Liu等, 2013)、石榴石的斑杂状显微结构(例如, Perchuk等, 2005, 2008)、长英质熔体薄膜和多硅白云母与石英之间的熔融反应结构(例如, Lang和Gilotti, 2007; Liu P L等, 2014)等(图2(d)~(f)). 这些显微地质证据是相对复杂的, 它们的岩石成因解释也是有争议的(例如, Zheng等, 2011), 还需要更进一步的部分熔融实验, 特别是低程度熔融实验和多晶包裹体的均一化实验来反演大陆俯冲带深部的熔/流体交代作用. 从来自大别-苏鲁造山带的部分熔融显微构造的证据来看, 超高压榴辉岩的部分熔融程度是很低的(例如, Gao等, 2012; Liu等, 2013; Liu P L等, 2014), 但花岗质片麻岩普遍经历了同折返部分熔融作用(例如, Wallis等, 2005; Zong等,
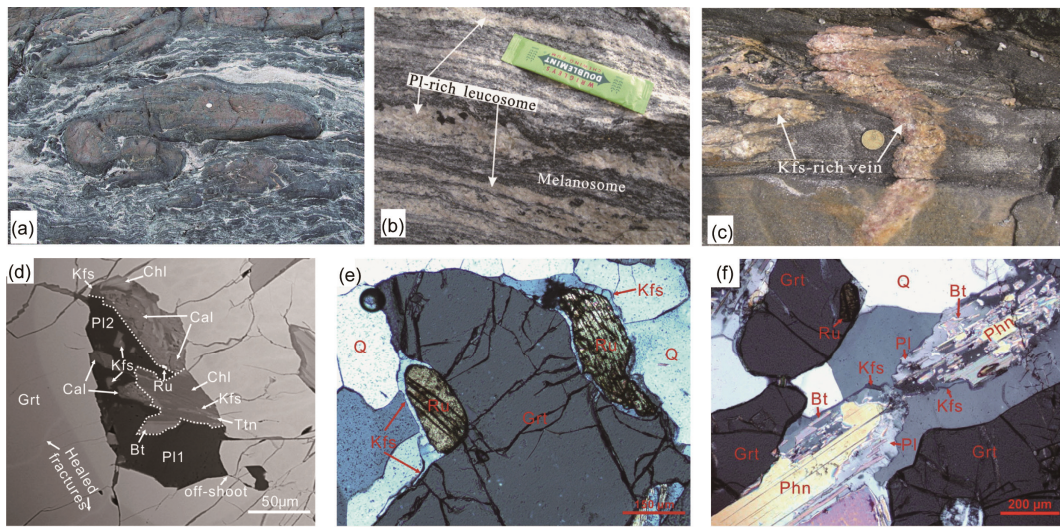
图 2　超高压岩石发生部分熔融的地质证据

苏鲁造山带仰口将军山地区发生了深熔作用的超高压榴辉岩(a); 苏鲁威海地区混合岩化片麻岩中富斜长石的浅色体、暗色体(b)和富钾长石的切割片麻岩面理的脉体(c); 大别造山带甘家岭地区钙质片麻岩中的长英质多相固体包体和石榴石的斑状结构(d)、金红石周边的钾长石薄膜(e)和多硅白云母与石英之间的熔融反应(f). 据 Wang 等(2014), Xu H J 等(2013)和 Liu P L 等(2014)

2010; Liu等, 2010, 2012; Chen等, 2013a, 2013b; Xu H J等, 2013). 这些熔/流体如果能够运移到上覆地幔楔中, 将在大陆俯冲带壳幔交换作用过程中起到重要作用(例如, Zheng, 2012; Zhao等, 2013; Zheng 和 Hermann, 2014).

3　大陆俯冲隧道中的壳幔相互作用

　　大别-苏鲁超高压变质带是由华南陆块向华北陆块俯冲至地幔至少100~200 km深度形成的典型陆-陆碰撞造山带(例如, Wang等, 1989; Xu等, 1992; Ye等, 2000). 已有的研究结果表明, 大别-苏鲁超高压变质带中的超高压变质岩在从地幔深度向上折返过程中在俯冲隧道内发生了显著的脱水和部分熔融作用, 形成富水流体和含水熔体(例如, Wallis等, 2005; Liu等, 2010; Gao等, 2012; Guo等, 2012; Chen等, 2013a, 2013b; Xu H J等, 2013; Song等, 2014a; Wang等, 2014), 特别是到达下地壳深度时这种退变质流体活动显著, 如果流体以弥散式流动则引起角闪岩相退变质, 如果发生局部聚集则形成石英脉(例如, Zheng, 2009). 这些熔/流体可以沿板片-地幔界面流动并上升进入上覆地幔楔, 富水流体的交代将主要形成蛇纹石化/绿泥石化/金云母化橄榄岩, 而熔体与地幔楔橄榄岩反应形成富化超镁铁质(二辉橄榄岩、辉石岩、

角闪岩)交代体(例如, Zhang等, 2005; Malaspina等, 2006, 2009; Zhang等, 2011; Zheng, 2012). 这些交代体可以在造山带岩石圈地幔中储存几个乃至几十个百万年, 在受到加热后发生部分熔融, 形成具有弧型微量元素特征和相对富集放射性成因Sr-Nd-Hf同位素特征的同折返碱性岩浆作用(例如, Chen等, 2003; 郭敬辉等, 2005; Yang等, 2005; 陈竟志和姜能, 2011; Zhao等, 2012; Xu等, 2015)或者碰撞后镁铁质岩浆作用(例如, Jahn等, 1999; Zhao等, 2011, 2013; Dai等, 2011, 2012; Xu等, 2012a; Yang D B等, 2012; Yang Q L等, 2012a, 2012b; Zhang J等, 2012).

　　在苏鲁造山带东部荣成地区发育的三叠纪晚期(~210 Ma)富钾的碱性杂岩, 碱性辉长岩、辉石正长岩、角闪石正长岩、石英正长岩和正长花岗岩, 其形成时代在超高压变质峰期(约238~227 Ma)(例如, Liu等, 2004, 2006, 2008, 2010; Zong等, 2010)之后约15~20 Myr, 为同折返或碰撞后岩浆作用, 原始基性岩浆可能来源于富化地幔, 认为是被俯冲的华南陆壳来源熔体交代的地幔楔橄榄岩部分熔融的结果(例如, Zhao等, 2012; Xu等, 2015). 在大别造山带的北大别地区发育的早白垩世(约130~120 Ma)辉长岩和辉石岩(例如, Jahn等, 1999; Dai等, 2011, 2012; Zhao等, 2011, 2013; Xu等, 2012a; Yang Q L等, 2012a, 2012b), 是碰撞后大陆造山带垮塌过程中的岩浆作用形成的

(Zhao等，2013)，具有弧型微量元素和富集放射成因Sr-Nd-Hf同位素的特征，这些镁铁质岩石的地幔源区也被认为是古老的岩石圈地幔受到俯冲陆壳来源熔体的交代(图3). 所不同的是，在晚三叠世被俯冲陆壳来源熔体交代了的地幔岩石，在造山带岩石圈地幔中储存了近100 Myr之后，在早白垩世造山带垮塌(例如，Xie等，2006; Wang等，2007; Xu等，2007, 2012a, 2012c)过程中发生部分熔融形成这些镁铁质岩石(例如，Jahn等，1999; Dai等，2011, 2012; Zhao等，2011，2013). 总的来说，大别-苏鲁超高压变质带中同碰撞和碰撞后岩浆侵入活动非常显著.

喜马拉雅造山带作为典型的弧-陆碰撞造山带，广泛发育同碰撞和碰撞后的新生代岩浆活动. 尤其是位于拉萨地块南部的冈底斯带，记录了从新特提斯洋开始向北与欧亚板块发生俯冲消减、印度板块与欧亚大陆碰撞并发生大陆俯冲以来的各种岩浆活动(例如，Royden等，2008). 前人研究表明，冈底斯岩基新生代岩浆活动主要为: (1) 65~41 Ma的林子宗火山岩和同期的冈底斯岩基岩浆侵入活动(例如，Wen等，2008; Mo等，2008; Ji等，2009); (2) 26~8 Ma的埃达克质斑岩(例如，Chung等，2003; Hou等，2004; Qu等，2004; Gao等，2007; Guo等，2007; Xu等，2009)和钾质-超钾质火山岩(Nomade等，2004; 赵志丹等，2006; 陈建林等，2007; Zhao等，2009). 前者被认为主要与新特提斯洋壳俯冲、板片后撤和断离等一系列复杂地质过程有关，并存在与俯冲、碰撞相关的岩浆底侵事件

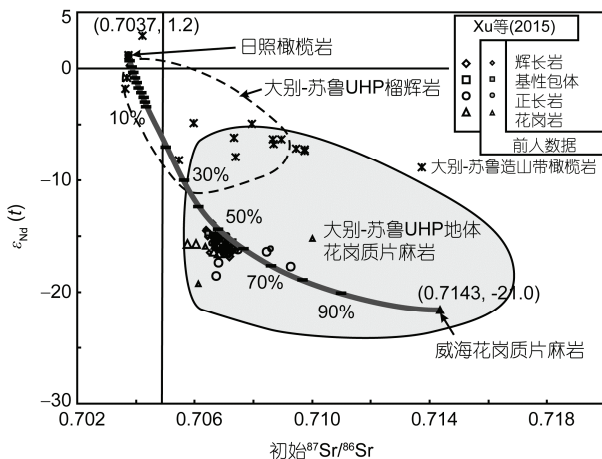**图 3 苏鲁造山带东部荣成地区晚三叠纪石岛碱性杂岩 Sr-Nd 同位素图解**

石岛杂岩的 Sr-Nd 同位素比值介于造山带橄榄岩和花岗质片麻岩之间，指示熔体交代了地幔橄榄岩. 数据来自 Xu 等(2015)

和壳幔岩浆混合作用. 后者形成了规模较小但分布广泛的钾质-超钾质岩，被认为是高原垮塌的标志. 同期在冈底斯出现大量岩株状侵入的埃达克质斑岩，被认为是加厚下地壳直接熔融的结果(Chung等，2003; Hou等，2004)，但也有研究认为其形成可能与俯冲或残留的洋壳熔融、交代地幔的熔融(Gao等，2007; Qu等，2004)或俯冲的印度下地壳部分熔融(Xu等，2009)有关.

上述研究表明，大陆俯冲隧道中早期洋壳或后期陆壳来源熔体对上覆地幔楔的交代作用，是大陆深俯冲过程中壳幔交换作用的重要过程. 大陆碰撞造山带中出露的同折返或碰撞后镁铁质岩浆岩代表了壳幔相互作用产物，对认识造山带地壳再循环和壳幔相互作用的过程和机制、熔/流体性质和被交代的地幔属性具有重要意义.

4 部分熔融和壳幔相互作用实验研究

要正确认识和解释俯冲隧道中复杂的部分熔融和壳幔相互作用现象，离不开高温高压实验的制约. 本节综述了硅酸盐和碳酸盐岩石的部分熔融和熔体与橄榄岩反应的实验研究进展.

4.1 部分熔融实验

4.1.1 硅酸盐岩石

部分熔融实验研究结果表明，基性硅酸盐岩石(角闪岩和玄武岩类)在低压条件下($P \leqslant 10$ kbar)发生部分熔融，形成的残余相矿物组合为富钙的斜长石+角闪石+单斜辉石±斜方辉石±石英±钛铁矿(Beard和Lofgren，1991; Wolf和Wyllie，1994; Rapp和Watson，1995; Patiño Douce和Beard，1995; Springer和Seck，1997); 而在压力为12.5~15 kbar条件下，基性岩石发生部分熔融形成的残余相矿物组合则以石榴石+单斜辉石+富钠的斜长石±角闪石为主(Sen和Dunn，1994a; Patiño Douce，2005; Rapp和Watson，1995; Skjerlie和Johnston，1996; Springer和Seck，1997; Skjerlie和Patiño Douce，2002; Qian和Hermann，2013). 在更高的压力条件下(15~30 kbar)，形成的残留体以石榴石+单斜辉石为主，斜长石消失(Sen和Dunn，1994b; Rapp和Watson，1995; Skjerlie和Patiño Douce，2002). 不论残留相具有什么样的矿物组合，地壳岩石部分熔融产生的熔体成分总是长英质的，除非岩石中的镁铁

质含水矿物优先熔融产生镁铁质熔体.

与基性岩类似, 中酸性硅酸盐岩部分熔融产生的残留体的矿物组成也随着温压条件的改变而变化. 在低压条件下(P≤10 kbar)中酸性岩部分熔融的残余相的典型矿物组合为富钙的斜长石+石英+斜方辉石+钛铁矿±黑云母(Patiño Douce 和 Beard, 1995); 在压力为12.5~15 kbar条件下残余相矿物组合为石榴石+单斜辉石+石英+斜长石±斜方辉石±钾长石(Patiño Douce 和 Beard, 1995; Skjerlie 和 Johnston, 1996; Litvinovsky等, 2000; Patiño Douce, 2005); 在更高的压力条件下(15~32 kbar)形成石榴石+单斜辉石+金红石+石英/柯石英±富钠的斜长石为主的残余相矿物组合 (Skjerlie 和 Johnston, 1996; Litvinovsky 等, 2000; Patiño Douce, 2005). 但中酸性岩(英云闪长质-花岗闪长质组分)部分熔融产生的熔体主要为花岗质.

因此, 在压力低于10 kbar (~30 km)条件下, 无论是基性岩还是中酸性岩发生部分熔融, 残余相中都大量存在富钙的斜长石, 缺乏石榴石和金红石, 与此平衡的花岗质熔体应具明显的负Eu异常、平坦的HREE分配模式和低的 Sr/Y 和 La/Yb 比值 (Rapp 等, 1999; Springer和Seck, 1997), 这是典型的非埃达克质花岗岩的成分特征. 在压力高于15 kbar(~50 km)条件下, 基性岩和中酸性岩部分熔融残余相中均富含石榴石和金红石, 斜长石消失或者变为富钠的斜长石, 与之平衡的花岗质熔体应具有强烈富集LREE、亏损HREE、高La/Yb比值、亏损HFSE、高Sr、低Y、高Sr/Y比值、没有明显的Eu异常等与埃达克岩类似的成分特征(Rapp等, 1999; Sen和Dunn, 1994a; Springer和Seck, 1997; Litvinovsky等, 2000; Xiong等, 2005). 无论是基性岩体系还是中酸性岩体系, 部分熔融发生的深度控制着熔体和残留体的地球化学组成. 具有埃达克岩性质的花岗质岩石被认为是典型的高压(>50 km)部分熔融的产物, 而不具有埃达克岩性质的花岗质岩石被认为典型的中低压部分熔融的产物, 它们具有明确的深度和构造指示意义.

4.1.2 碳酸盐岩石

碳酸盐岩($CaCO_3$, $MgCO_3$, $FeCO_3$)是俯冲带中一种重要的岩石类型, 可以被俯冲带入地球深部参与碳循环过程(例如, Dasgupta和Hirschmann, 2010). 前人实验研究表明, 纯碳酸盐岩在地球内部高温高压条件下可以一直稳定地存在到至少300 km的深度,

需要较高的温度(>1300℃)才能发生熔融(例如, Irving和Wyllie, 1975; Ivanov和Deutsch, 2002; Tao等, 2013). 对干的碳酸盐化橄榄岩和碳酸盐化榴辉岩的部分熔融实验研究证实, 它们可以形成白云石质的碳酸盐熔体, 其固相线温度受控于压力和全岩成分(Na_2O/CO_2和CaO/MgO), 高于俯冲带在上地幔300 km深度范围内的温度(例如, Dalton和Presnall, 1998; Dasgupta等, 2004, 2005; Yaxley和Brey, 2004; Gudfinnsson和Presnall, 2005; Brey等, 2008, 2009; Foley等, 2009; Girnis等, 2011). 碳酸盐熔体中SiO_2含量随温度升高增加, 由碳酸盐熔体向碳酸盐化硅酸盐熔体转变(例如, Hirose, 1997; Dalton和Presnall, 1998; Dasgupta和Hirschmann, 2006; Dasgupta等, 2013)(图4). 微量(100 ppm)CO_2即可有效降低橄榄岩的熔点130~140℃; 当CO_2和H_2O同时存在时, 由于H_2O在熔体中比名义上无水矿物中更高的分配系数, 对橄榄岩熔点的降低作用可能会更加显著(Dasgupta等, 2007a, 2007b). 俯冲带中富水的碳酸盐化泥质岩在>5~7 GPa条件下具有最低的熔点, 比周边地幔温度低200~400℃, 在地幔中存储足够长的时间就会发生部分熔融形成熔体. 前人研究表明, 具有1.1 wt%水的碳酸盐在8~14 GPa条件下的初熔温度要比干条件下低100~150℃(Grassi和Schmidt, 2011; Grassi等,
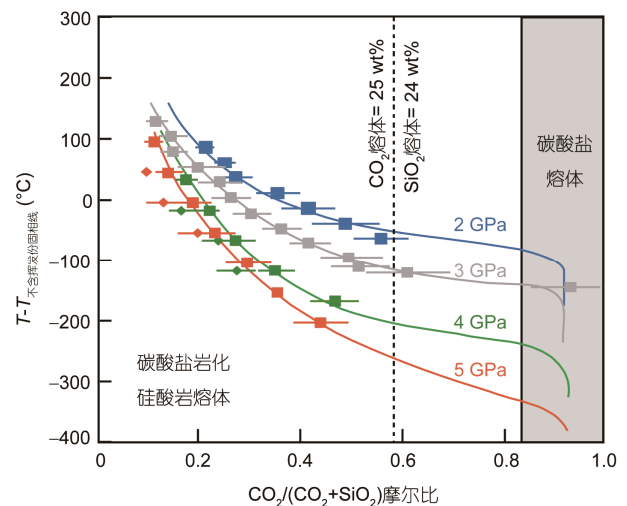

图 4　碳酸盐熔体成分随温度和压力的变化

实验数据表明碳酸盐化硅酸盐岩的初始熔融温度比不含挥发份的硅酸岩低, 并随压力增加熔点降低程度更大; 另外, 碳酸盐熔体与碳酸盐化硅酸盐熔体之间的转化在低压(<3 GPa)下非常迅速, 在高压下是渐变的. 数据来自 Dasgupta 等(2013)

2012), 仅仅0.1%的碳酸盐熔体就可以萃取岩石体系中30%~60%的不相容微量元素(Klemme等, 1995; Sweeney等, 1995; Blundy和Dalton, 2000; Brey等, 2008; Girnis等, 2006; Dasgupta等, 2009).

4.2 熔体-橄榄岩反应实验

4.2.1 硅酸盐熔体

Nicholls等(1973)最早提出, 俯冲洋壳在俯冲带100~150 km深部脱水和部分熔融, 产生的富水熔体上升进入上覆地幔楔后, 将与地幔楔橄榄岩发生交代反应形成橄榄辉石岩, 这些交代体的部分熔融被认为导致了同俯冲岛弧岩浆作用. 围绕大洋俯冲带中的熔/流体与橄榄岩反应的高温高压实验研究工作已经很多, 根据与橄榄岩反应的岩石性质分类, 包括有合成或天然中酸性富水长英质岩石(花岗岩、英云闪长岩、花岗闪长岩、TTG)(Sekine和Wyllie, 1982a, 1982b, 1983; Wyllie和Sekine, 1982; Wyllie等, 1989; Carroll和Wyllie, 1989; Rapp等, 2010)和基性岩石(MORB、角闪岩、榴辉岩、角闪石化枕状熔岩、安山岩)(Sen和Dunn, 1994b; Kogiso等, 1998; Rapp等, 1999, 2010; Yaxley, 2000; Mallik和Dasgupta, 2012, 2013). 富水长英质岩石与橄榄岩反应主要产物是含金云母和石榴石的二辉石岩(Sekine和Wyllie, 1982a, 1982b, 1983; Wyllie和Sekine, 1982; Wyllie等, 1989; Carroll和Wyllie, 1989), 而基性岩石与橄榄岩反应的产物比较复杂, 包括石榴辉石岩、橄榄角闪岩/辉石岩、石榴二辉橄榄岩等(Sen和Dunn, 1994b; Kogiso等, 1998; Rapp等, 1999; Yaxley, 2000; Rapp等, 2010; Mallik和Dasgupta, 2012), 由反应物所衍生的熔体包括高镁埃达克岩(Rapp等, 1999)、富Fe-Ti的洋岛型玄武岩(Kogiso等, 1998; Mallik和Dasgupta, 2012; Yaxley, 2000)或各种原生碱性玄武岩(Mallik和Dasgupta, 2013). 实验产物成分是由实验初始矿物和化学成分、熔融程度、熔体与橄榄岩比例共同决定的. 榴辉岩、安山岩和玄武岩产生的部分熔体与橄榄岩之间的反应会形成反应分带现象, 在橄榄岩不发生部分熔融的相对低温条件下榴辉岩端元形成石榴辉石岩和熔体, 反应过渡带为(石榴)二辉石岩(图5(a))(王超等, 2010; Zhang J F等, 2012), 更高温度下橄榄岩也可形成纯橄榄-方辉橄榄岩-二辉橄榄岩带(Wang等, 2013)(图5(b)). Zhang J F等(2012)通过对比静态和

变形条件下的熔体与橄榄岩之间的反应指出, 干体系下熔体-橄榄岩反应是一个非常缓慢的自我抑制过程, 需要变形来驱动才有可能产生相对较大范围的熔体-橄榄岩反应.

4.2.2 碳酸盐熔体

相比硅酸盐熔体, 碳酸盐熔体具有低密度、低粘度和高反应活性, 被认为是最有效的地幔交代介质(例如, Grassi和Schmidt, 2011; Grassi等, 2012). Martin等(2012)实验研究了6 GPa和900℃条件下白云石+柯石英与石榴二辉橄榄岩/方辉橄榄岩之间的反应, 其结果是形成了菱镁矿+相对富钙的单斜辉石和橄榄岩的碳酸盐化. 采用碳酸盐化蓝闪石片岩与纯橄榄岩反应的结果则主要在橄榄石区域消耗橄榄石形成了斜方辉石(Perchuk等, 2013; Perchuk和Yapaskurt, 2013). Bulatov等(2014)的进一步实验研究表明, 碳酸盐熔体与橄榄岩反应同样形成了反应条带(图5(c)), 在原橄榄岩区形成低Ca辉石石榴石岩, 在原沉积物区形成榴辉岩或碳酸盐化榴辉岩. 这些实验结果体现了Si组分由沉积物向橄榄岩运移而Mg, Fe组分向沉积物运移的元素迁移规律, 反应产生的熔体具有相比海底沉积物部分熔融熔体更高的Mg, Si含量和更低的Ca含量. Russell等(2012)认为地幔中存在硅饱和熔体和硅不饱和熔体, 后者的CO_2含量高, 相当于碳酸盐熔体(图6(a)); 碳酸盐熔体中CO_2的含量主要取决于熔体中$SiO_2+Al_2O_3$的含量, 碳酸盐熔体在地幔运移过程中会发生对斜方辉石的同化吸收, 使硅不饱和的碳酸盐岩浆中SiO_2含量增加, 导致CO_2在岩浆中的溶解度快速降低而出溶(图6(b)); 同时, CO_2的出溶或排气作用也有利于岩浆的底劈上侵穿过致密的岩石圈地幔, 这个反应过程还会导致初始流体相的橄榄石结晶分异作用(图6(c)).

4.3 壳幔相互作用过程中的熔体性质

可以推测, 熔体与橄榄岩反应方式可能主要有两种. 一种是硅饱和熔体与橄榄岩反应, 通过消耗橄榄石形成斜方辉石和单斜辉石, 反应产物主要是富化的二辉橄榄岩(+石榴辉石岩残余), 这个反应过程往往在橄榄石和斜方辉石周边形成致密、隔离熔体的反应边(图7(a)), 使熔体与橄榄岩反应很难继续进行下去, 熔体被局限在熔体通道中由浮力作用上升运移. 另一种是硅不饱和熔体与橄榄岩反应, 通过消耗
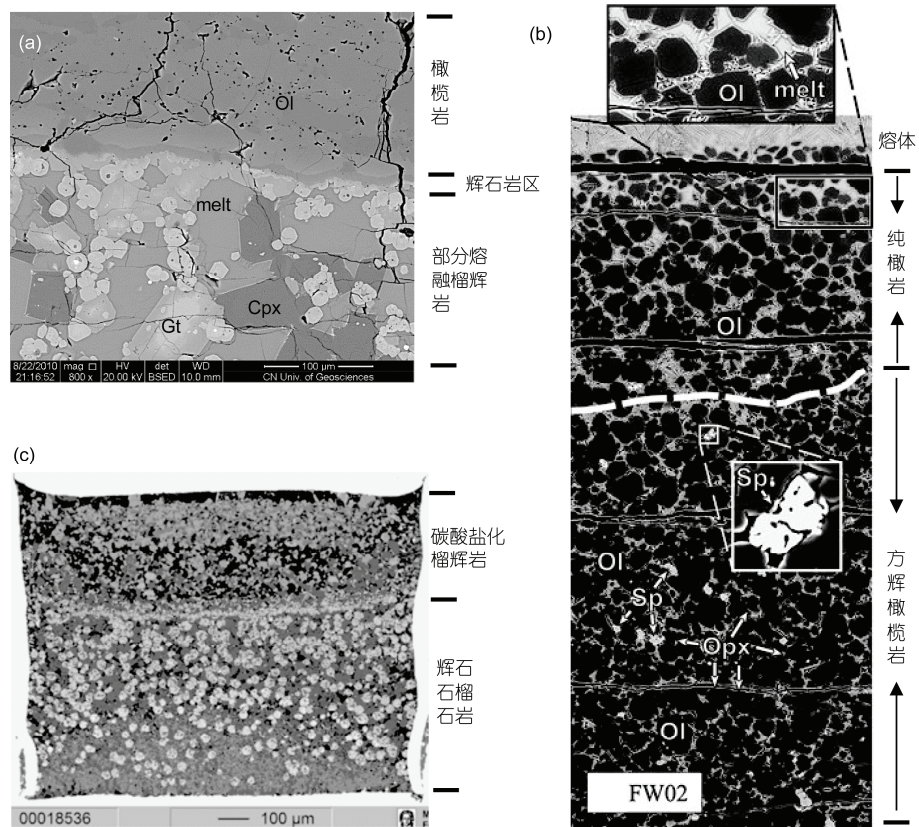
图 5　不同性质的硅酸盐熔体与橄榄岩反应的结果

(a) 榴辉岩熔体与橄榄岩反应形成薄的致密辉石岩层(1250℃, 2 GPa); (b) 玄武岩熔体与橄榄岩反应形成纯橄榄岩和方辉橄榄岩(1425℃, 2 GPa); (c) 碳酸盐沉积物与橄榄岩反应在原橄榄岩区形成的低 Ca 辉石石榴石岩, 在原沉积物区形成榴辉岩或碳酸盐化榴辉岩(1100℃, 7.1 GPa). 数据来自 Zhang J F 等(2012), Wang 等(2013)和 Bulatov 等(2014)

斜方辉石形成橄榄石, 反应产物主要是富化的异剥橄榄岩, 这个反应过程通过蚕食斜方辉石形成疏松的橄榄岩, 为熔体在橄榄岩中大规模运移和参与与橄榄岩反应提供通道(图7(b), (c)), 但随着反应的不断进行, 如果熔体得不到及时补充, 熔体吸收斜方辉石后将导致熔体中SiO_2组分含量的上升和C-O-H流体的不断析出, 最终硅不饱和熔体转化为硅饱和熔体, 继续和橄榄岩发生交代作用直至熔体消耗完毕或运移至地表附近.

5　研究意义和展望

将俯冲隧道模型拓展到大陆碰撞造山带, 能够解析大陆俯冲带构造过程及其产物, 改变现行的地球动力学观, 为发展和完善板块构造理论提供新的科学依据. 对陆壳深俯冲和折返过程以及大陆俯冲

隧道内不同类型深俯冲板片与地幔楔岩石相互作用的深入研究, 无疑将是认识和发展俯冲隧道模型的关键. 通过过去几十年对大陆造山带的不断研究, 我们对造山带的构造演化过程的理论认识不断深入, 大陆俯冲隧道过程(Zheng, 2012; 郑永飞等, 2013)可以合理解释超高压变质岩产出、碰撞造山带的类型、超高压变质地体的大小和折返速率等大陆造山带过程关键基础科学问题, 进一步丰富和发展了板块构造和大陆动力学基础理论. 而有关深俯冲大陆地壳的再循环、部分熔融和壳幔交换仍旧是壳幔相互作用研究中未解决的难点和关键科学问题. 相关的高温高压实验研究将为进一步完善和发展这一理论提供重要的实验依据和约束.

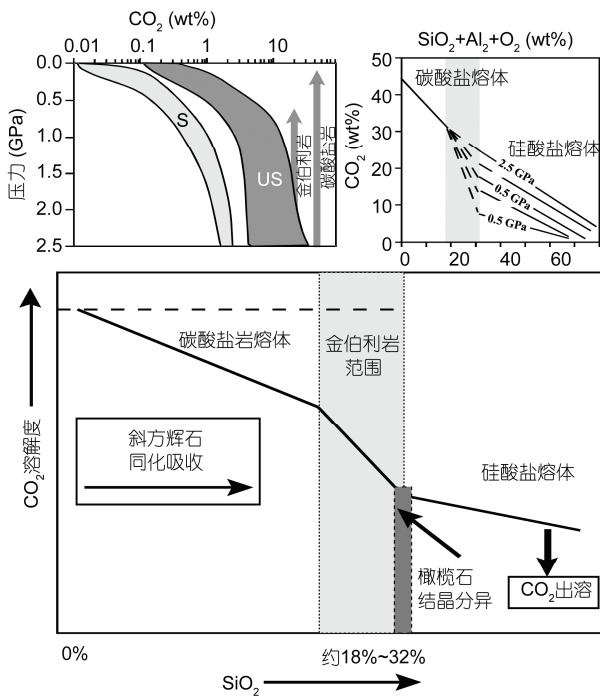相对大洋俯冲隧道, 一方面卷入大陆俯冲隧道的物质成分非常复杂, 既有俯冲洋壳的玄武岩、辉长岩和大洋沉积物, 也有俯冲陆壳的基底花岗岩、麻粒

图6　CO_2在硅酸盐和碳酸盐熔体中的溶解度

(a) 硅饱和熔体(S)和硅不饱和熔体(US)中 CO_2 的溶解度; (b) 碳酸盐熔体与硅酸盐熔体中 CO_2 溶解度随压力的变化; (c) 碳酸盐熔体在地幔中逐步演化变成硅酸盐熔体过程的示意图. 数据来自Russell等(2012)

岩以及沉积盖层; 另一方面大陆俯冲带岩石圈地幔楔具有低温度和低水活度的特点(Zheng和Hermann, 2014). 由于大陆岩石圈与大洋岩石圈在物质组成和状态上的显著差异, 其深部物理和化学过程及壳幔相互作用产物必然出现一系列差异. 已有研究表明,

来自大陆俯冲带片麻岩的流体可能是一种对Hf和O有较强迁移能力的含水熔体, 而来自榴辉岩的流体是一种仅对O有较强的迁移能力的含水流体(例如, Liu X C等, 2014). 因此, 从高温高压实验的角度, 需要充分考虑板片-地幔界面上各种不同地壳成分及其衍生的熔/流体成分与不同橄榄岩之间的复杂反应过程及产物. 存在的科学问题包括: (1) 牵引大陆地壳深俯冲的古洋壳与上覆地幔楔橄榄岩发生交代作用的条件、机制和产物是什么? (2) 大陆俯冲带深部发生变质脱水、部分熔融、地幔交代的条件、机制和产物是什么? (3) 折返过程中不同成分大陆俯冲带物质所形成的部分熔融熔体的特征及其在折返过程中所起到的作用是什么?

这些关键科学问题的理解和解释, 离不开对俯冲带岩石中记录的壳幔相互作用的研究和高温高压实验研究的验证和制约. 俯冲隧道概念在大陆俯冲中的应用才刚刚开始, 相关可供直接应用的高温高压实验研究结果非常有限, 已有的实验结果也主要是针对大洋岛弧环境条件而不是大陆俯冲带的环境.

高温高压实验在模拟地球内部相对真实温度和压力条件下的物理和化学过程具有不可替代的优势, 也是当今地球前沿研究领域. 因此, 瞄准大陆俯冲隧道中壳幔交换作用这一国际前沿关键问题, 以我国的秦岭-大别-苏鲁造山带和喜马拉雅造山带这两个独特的大陆动力学地质现象为依托, 开展大陆俯冲带壳幔相互作用过程的高温高压实验系统研究, 对获取国际领先水平的系统成果, 进一步发展大陆动力学理论具有重要的科学意义.
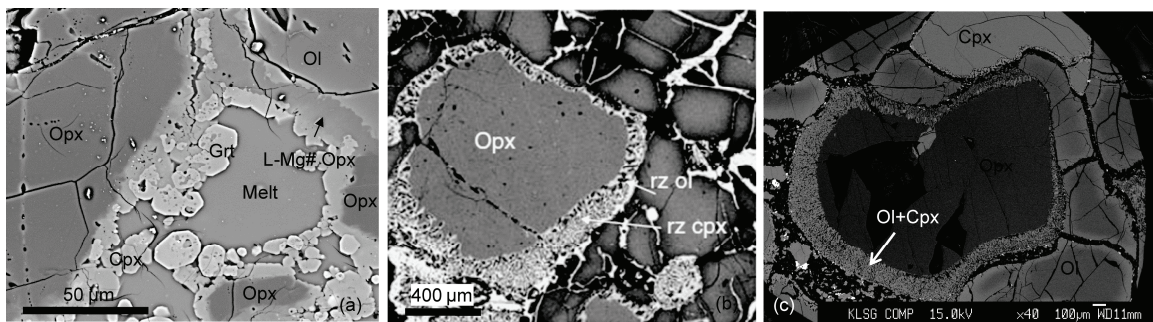

图7　硅饱和熔体和硅不饱和熔体与橄榄岩之间的反应

(a) 麻粒岩部分熔融形成的硅饱和熔体(melt)与橄榄岩反应形成围绕橄榄石(ol)和斜方辉石(opx)的致密低镁值斜方辉石(L-Mg$^\#$ opx)和单斜辉石(cpx)反应边(实验条件为2 GPa, 1300℃, 48 h); (b) 硅不饱和熔体(白榴岩)与橄榄岩反应形成围绕斜方辉石的筛状反应边(1 个大气压, 1200℃, 312 h); (c) 河北大麻坪橄榄岩中斜方辉石与硅不饱和熔体反应形成的筛状反应边. 数据来自王永锋等(2013)和Shaw等(2008)

参考文献

陈建林, 许继峰, 康志强, 王保弟. 2007. 青藏高原西南部查孜地区中新世钾质火山岩地球化学及其成因. 地球化学, 36: 437–447

陈竟志, 姜能. 2011. 胶东晚三叠世碱性岩浆作用的岩石成因——来自锆石U-Pb年龄、Hf-O同位素的证据. 岩石学报, 27: 3557–3574

郭敬辉, 陈福坤, 张晓曼, Siebel W, 翟明国. 2005. 苏鲁超高压带北部中生代岩浆侵入活动与同碰撞-碰撞后构造过程: 锆石U-Pb年代学. 岩石学报, 21: 1281–1301

刘福来, 薛怀民, 刘平华. 2009. 苏鲁超高压岩石部分熔融时间的准确限定: 来自含黑云母花岗岩中锆石U-Pb定年、REE和Lu-Hf同位素的证据. 岩石学报, 25: 1039–1055

王超, 金振民, 高山, 章军锋, 郑曙. 2010. 华北克拉通岩石圈破坏的榴辉岩熔体-橄榄岩反应机制: 实验约束. 中国科学: 地球科学, 40: 541–555

王永锋, 章军锋. 2013. 斜方辉石筛状反应边的成因机制及其对岩石圈地幔性质转变的意义. 岩石矿物学杂志, 32: 604–612

赵志丹, 莫宣学, Nomade S, Renne P R, 周肃, 董国臣, 王亮亮, 朱弟成, 廖忠礼. 2006. 青藏高原拉萨地块碰撞后超钾质岩石的时空分布及其意义. 岩石学报, 22: 787–794

赵子福, 郑永飞. 2009. 俯冲大陆岩石圈重融: 大别-苏鲁造山带中生代岩浆岩成因. 中国科学D辑: 地球科学, 39: 888–909

曾令森, 高丽娥, 于俊杰, 胡古月. 2011. 苏鲁仰口超高压岩石SHRIMP锆石U/Pb定年与部分熔融时限. 岩石学报, 27: 1085–1094

曾令森, 梁凤华, Asimow P, 陈方远, 陈晶. 2009. 深俯冲陆壳岩石部分熔融与苏鲁超高压榴辉岩中长英质多晶包裹体的形成. 科学通报, 54: 1826–1840

郑永飞, 赵子福, 陈伊翔. 2013. 大陆俯冲隧道过程: 大陆碰撞过程中的板片界面相互作用. 科学通报, 58: 2233–2239

Allègre C J. 1982. Chemical geodynamics. Tectonophysics, 81: 109–132

Auzanneau E, Vielzeuf D, Schmidt M W. 2006. Experimental evidence of decompression melting during exhumation of subducted continental crust. Contrib Mineral Petrol, 152: 125–148

Beard J S, Lofgren G E. 1991. Dehydration melting and water-saturated melting of basaltic and andesitic greenstones and amphibolites at 1, 3, and 6.9 kbar. J Petrol, 32: 365–401

Beaumont C, Ellis S, Pfiffner A. 1999. Dynamics of sediment subduction-accretion at convergent margins: Short-term modes, long-term deformation, and tectonic implications. J Geophys Res, 104: 17573–17601

Beaumont C, Jamieson R A, Butler J P, Warren C J. 2009. Crustal structure: A key constraint on the mechanism of ultra-high-pressure rock exhumation. Earth Planet Sci Lett, 287: 116–129

Bebout G E. 2007. Metamorphic chemical geodynamics of subduction zones. Earth Planet Sci Lett, 260: 373–393

Bercovici D, Karato S. 2003. Whole-mantle convection and the transition-zone water filter. Nature, 425: 39–44

Blundy J, Dalton J. 2000. Experimental comparison of trace element partitioning between clinopyroxene and melt in carbonate and silicate systems, and implications for mantle metasomatism. Contrib Mineral Petrol, 139: 356–371

Brey G P, Bulatov V K, Girnis A V, Lahaye Y. 2008. Experimental melting of carbonated peridotite at 6–10 GPa. J Petrol, 49: 797–821

Brey G P, Bulatov V K, Girnis A V. 2009. Influence of water and fluorine on melting of carbonated peridotite at 6 and 10 GPa. Lithos, 112: 249–259

Bulatov V K, Brey G P, Girnis A V, Gerdes A, Höfer H E. 2014. Carbonated sediment-peridotite interaction and melting at 7.5–12 GPa. Lithos, 200–201: 368–385

Carroll M R, Wyllie P J. 1989. Granite melt convecting in an experimental micro-magma chamber at 1050°C, 15 kbar. Eur J Mineral, 1: 249–260

Chen J F, Xie Z, Li H M, Zhang X D, Zhou T X, Park Y S, Ahn K S, Chen D G, Zhang X. 2003. U-Pb zircon ages for a collision-related K-rich complex at Shidao in the Sulu ultrahigh pressure terrane. China Geochem J, 37: 35–46

Chen Y X, Zheng Y F, Hu Z C. 2013a. Petrological and zircon evidence for anatexis of UHP quartzite during continental collision in the Sulu orogen. J Metamorphic Geol, 31: 389–413

Chen Y X, Zheng Y F, Hu Z C. 2013b. Synexhumation anatexis of ultrahigh-pressure metamorphic rocks: Petrological evidence from granitic gneiss in the Sulu orogen. Lithos, 156–159: 69–96

Chen Y X, Zheng Y F, Gao X Y, Hu Z C. 2014. Multiphase solid inclusions in zoisite-bearing eclogite: Evidence for partial melting of ultrahigh-pressure metamorphic rocks during continental collision. Lithos, 200–201: 1–21

Chopin C. 2003. Ultrahigh-pressure metamorphism: Tracing continental crust into the mantle. Earth Planet Sci Lett, 212: 1–14

Chung S L, Liu D Y, Ji J Q, Chu M F, Lee H Y, Wen D J, Lo C H, Lee T Y, Qian Q, Zhang Q. 2003. Adakites from continental collision zones: Melting of thickened lower crust beneath southern Tibet. Geology, 31: 1021–1024

Cloos M, Shreve R L. 1988a. Subduction-channel model of prism accretion, mélange formation, sediment subduction, and subduction erosion at convergent plate margins: 1, Background and description. Pure Appl Geophys, 128: 455–500

Cloos M, Shreve R L. 1988b. Subduction-channel model of prism accretion, mélange formation, sediment subduction, and subduction erosion at convergent plate margins: 2, Implications and discussion. Pure Appl Geophys, 128: 501–505

Dai L Q, Zhao Z F, Zheng Y F, Li Q L, Yang Y H, Dai M N. 2011. Zircon Hf-O isotope evidence for crust-mantle interaction during continental deep subduction. Earth Planet Sci Lett, 308: 224–244

Dai L Q, Zhao Z F, Zheng Y F, Zhang J. 2012. The nature of orogenic lithospheric mantle: Geochemical constraints from postcollisional mafic-ultramafic rocks in the Dabie orogen. Chem Geol, 334: 99–121

Dai L Q, Zhao Z F, Zheng Y F. 2015. Tectonic development from oceanic subduction to continental collision: Geochemical evidence from

postcollisional mafic rocks in the Hong'an-Dabie orogens. Gondwana Res, 27: 1236–1254

Dalton J A, Presnall D C. 1998. The continuum of primary carbonatitic-kimberlitic melt compositions in equilibrium with lherzolite: Data from the system $CaO-MgOAl_2O_3-SiO_2-CO_2$ at 6 GPa. J Petrol, 39: 1953–1964

Dasgupta R, Hirschmann M M, Withers A C. 2004. Deep global cycling of carbon constrained by the solidus of anhydrous, carbonated eclogite under upper mantle conditions. Earth Planet Sci Lett, 227: 73–85

Dasgupta R, Hirschmann M M, Dellas N. 2005. The effect of bulk composition on the solidus of carbonated eclogite from partial melting experiments at 3 GPa. Contrib Mineral Petrol, 149: 288–305

Dasgupta R, Hirschmann M M. 2006. Melting in the Earth's deep upper mantle caused by carbon dioxide. Nature, 440: 659–662

Dasgupta R, Hirschmann M M, Smith N D. 2007a. Partial melting experiments of peridotite+CO_2 at 3 GPa and genesis of alkalic ocean island basalts. J Petrol, 48: 2093–2124

Dasgupta R, Hirschmann M M, Smith N D. 2007b. Water follows carbon: CO_2 incites deep silicate melting and dehydration beneath mid-ocean ridges. Geology, 35: 135–138

Dasgupta R, Hirschmann M M, McDonough W F, Spiegelman M, Withers A C. 2009. Trace element partitioning between garnet lherzolite and carbonatite at 6.6 and 8.6 GPa with applications to the geochemistry of the mantle and of mantle derived melts. Chem Geol, 262: 57–77

Dasgupta R, Hirschmann M M. 2010. The deep carbon cycle and melting in Earth's interior. Earth Planet Sci Lett, 298: 1–13

Dasgupta R, Mallik A, Tsuno K, Withers A C, Hirth G, Hirschmann M M. 2013. Carbon-dioxide-rich silicate melt in the Earth's upper mantle. Nature, 493: 211–215

Foley S F, Yaxley G M, Rosenthal A, Buhre S, Kiseeva E S, Rapp R P, Jacob D E. 2009. The composition of near-solidus melts of peridotite in the presence of CO_2 and H_2O between 40 and 60 kbar. Lithos, 112S: 274–283

Gao X Y, Zheng Y F, Chen Y X. 2012. Dehydration melting of ultrahigh-pressure eclogite in the Dabie orogen: Evidence from multiphase solid inclusions in garnet. J Metamorphic Geol, 30: 193–212

Gao X Y, Zheng Y F, Chen Y X, Hu Z. 2013. Trace element composition of continentally subducted slab-derived melt: insight from multiphase solid inclusions in ultrahigh-pressure eclogite in the Dabie orogen. J Metamorphic Geol, 31: 453–468

Gao Y F, Hou Z Q, Kamber B S, Wei R H, Meng X J, Zhao R S. 2007. Adakite-like porphyries from the southern Tibetan continental collision zones: Evidence for slab melt metasomatism. Contrib Mineral Petrol, 153: 105–120

Gerya T V, Stöckhert B, Perchuk A L. 2002. Exhumation of high-pressure metamorphic rocks in a subduction channel: A numerical simulation. Tectonics, 21: 1056, doi: 10.1029/2002TC001406

Girnis A V, Bulatov V K, Lahaye Y, Brey G P. 2006. Partitioning of trace elements between carbonate-silicate melts and mantle minerals: Experiment and petrological consequences. Petrology, 14: 492–514

Girnis A V, Bulatov V K, Brey G P. 2011. Formation of primary kimberlite melts-constraints from experiments at 6–12 GPa and variable CO_2/H_2O. Lithos, 127: 401–413

Gordon S M, Whitney D L, Teyssier C, Fossen H. 2013. U-Pb dates and trace-element geochemistry of zircon from migmatite, Western Gneiss Region, Norway: Significance for history of partial melting in continental subduction. Lithos 170–171: 35–53

Grassi D, Schmidt M W. 2011. The melting of carbonated pelites from 70 to 700 km depth. J Petrol, 52: 765–789

Grassi D, Schmidt M W, Günther D. 2012. Element partitioning during carbonated pelite melting at 8, 13 and 22 GPa and the sediment signature in the EM mantle components. Earth Planet Sci Lett, 327–328: 84–96

Gudfinnsson G H, Presnall D C. 2005. Continuous gradations among primary carbonatitic, kimberlitic, melilititic, basaltic, picritic, and komatiitic melts in equilibrium with garnet lherzolite at 3–8 GPa. J Petrol, 46: 1645–1659

Guillot S, Hattori K, Agard P, Schwartz S, Vidal O. 2009. Exhumation processes in oceanic and continental subduction contexts: A review. In: Lallemand S, Funiciello F, eds. Subduction Zone Geodynamics. Berlin: Springer-Verlag. 175–205

Guo S, Ye K, Chen Y, Liu J, Mao Q, Ma Y. 2012. Fluid-rock interaction and element mobilization in UHP metabasalt: Constraints from an omphacite-epidote vein and host eclogites in the Dabie orogen. Lithos, 136–139: 145–167

Guo Z F, Wilson M, Liu J Q. 2007. Post-collisional adakites in south Tibet: Products of partial melting of subduction-modified lower crust. Lithos, 96: 205–224

Hermann J. 2002. Experimental constraints on phase relations in subducted continental crust. Contrib Mineral Petrol, 143: 219–235

Hermann J, Spandler C, Hack A, Korsakov A V. 2006. Aqueous fluids and hydrous melts in high-pressure and ultra-high pressure rocks: Implications for element transfer in subduction zones. Lithos, 92: 399–417

Hermann J, Zheng Y F, Rubatto D. 2013. Deep Fluids in Subducted Continental Crust. Elements, 9: 281–287

Hermann J, Rubatto D. 2014. Subduction of Continental Crust to Mantle Depth. In: Holland H D, Turekian K K, eds. Treatise on Geochemistry: Geochemistry of Ultrahigh-Pressure Rocks. Amsterdam: Elsevier. 309–340

Hirose K. 1997. Partial melt compositions of carbonated peridotite at 3 GPa and role of CO_2 in alkali-basalt magma generation. Geophys Res Lett, 24: 2837–2840

Hou Z Q, Gao Y F, Qu X M, Rui Z Y, Mo X X. 2004. Origin of adakitic intrusives generated during mid-Miocene east-west extension in southern Tibet. Earth Planet Sci Lett, 220: 139–155

Hwang S L, Shen P Y, Yui T F, Chu H T. 2003. Metal-sulfur-COH-silicate fluid mediated diamond nucleation in Kokchetav ultrahigh-pressure gneiss. Eur J Mineral, 15: 503–511

Irving A J, Wyllie P J. 1975. Subsolidus and melting relationships for calcite, magnesite and join $CaCO_3$-$MgCO_3$ to 36 kbar. Geochim Cosmochim Acta, 39: 35–53

Ivanov B A, Deutsch A. 2002. The phase diagram of $CaCO_3$ in relation to shock compression and decomposition. Phys Earth Planet Int, 129:

131–143

Jahn B M, Wu F, Lo C H, Tsai C H. 1999. Crust-mantle interaction induced by deep subduction of the continental crust: Geochemical and Sr-Nd isotopic evidence from post-collisional mafic-ultramafic intrusions of the northern Dabie complex, central China. Chem Geol, 157: 119–146

Ji W Q, Wu F Y, Chung S L, Li J X, Liu C Z. 2009. Zircon U-Pb geochronology and Hf isotopic constraints on petrogenesis of the Gangdese batholith, southern Tibet. Chem Geol, 262: 229–245

Klemme S, van der Laan S R, Foley S F, Günther D. 1995. Experimentally determined trace and minor element partitioning between clinopyroxene and carbonatite melt under upper-mantle conditions. Earth Planet Sci Lett, 133: 439–448

Kogiso T, Hirose K, Takahashi E. 1998. Melting experiments on homogeneous mixtures of peridotite and basalt: Application to the genesis of ocean island basalts. Earth Planet Sci Lett, 162: 45–61

Korsakov A V, Hermann J. 2006. Silicate and carbonate melt inclusions associated with diamonds in deeply subducted carbonate rocks. Earth Planet Sci Lett, 241: 104–118

Labrousse L, Prouteau G, Ganzhorn A C. 2011. Continental exhumation triggered by partial melting at ultrahigh pressure. Geology, 39: 1171–1174

Lang H M, Gilotti J A. 2007. Partial melting of metapelites at ultrahigh-pressure conditions, Greenland Caledonides. Contrib Mineral Petrol, 25: 129–147

Litvinovsky B A, Steele I M, Wickham S M. 2000. Silicic magma formation in overthickened crust: Melting of charnockite and leucogranite at 15, 20 and 25 kbar. J Petrol, 41: 717–737

Liou J G, Ernst W G, Zhang R Y, Tsujimori T, Jahn B M. 2009. Ultrahihg-pressure minerals and metamorphic terranes-The view from China. J Asian Earth Sci, 35: 199–231

Liu F L, Xu Z Q, Liou J G, Song B. 2004. SHRIMP U-Pb ages of ultrahigh-pressure and retrograde metamorphism of gneisses, south-western Sulu terrane, eastern China. J Metamorphic Geol, 22: 315–326

Liu F L, Gerdes A, Liou J G, Xue H M, Liang F H. 2006. SHRIMP U-Pb zircon dating from Sulu-Dabie dolomitic marble, South China: Constraints on prograde, ultrahigh-pressure and retrograde metamorphic ages. J Metamorphic Geol, 24: 569–589

Liu F L, Gerdes A, Zeng L S, Xue H. 2008. SHRIMP U-Pb dating, trace elements and the Lu-Hf isotope system of coesite-bearing zircon from amphibolite in the SW Sulu UHP terrane, eastern China. Geochim Cosmochim Acta, 72: 2973–3000

Liu F L, Robinson P T, Gerdes A, Xue H, Liu P, Liou J G. 2010. Zircon U-Pb ages, REE concentrations and Hf isotope compositions of granitic leucosome and pegmatite from the north Sulu UHP terrane in China: constraints on the timing and nature of partial melting. Lithos, 117: 247–268

Liu F L, Robinson P T, Liu P H. 2012. Multiple partial melting events in the Sulu UHP terrane: Zircon U-Pb dating of granitic leucosomes within amphibolite and gneiss. J Metamorphic Geol, 30: 887–906

Liu P L, Wu Y, Liu Q, Zhang L, Jin Z. 2014. Partial melting of UHP calc-gneiss from the Dabie Mountains. Lithos, 192–195: 86–101

Liu P L, Wu Y, Chen Y, Zhang J, Jin Z. 2015. UHP impure marbles fromthe Dabie Mountains: Metamorphic evolution and carbon cycling in continental subduction zones. Lithos, 212–215: 280–297

Liu Q, Hermann J, Zhang J F. 2013. Polyphase inclusions in the Shuanghe UHP eclogites formed by subsolidus transformation and incipient melting during exhumation of deeply subducted crust. Lithos, 177: 91–109

Liu X C, Wu Y B, Gao S, Wang H, Zheng J P, Hu Z C, Zhou L, Yang S H. 2014. Record of multiple stage channelized fluid and melt activities in deeply subducted slab from zircon U-Pb age and Hf-O isotope compositions. Geochim Cosmochim Acta, 144: 1–24

Malaspina N, Hermann J, Scambelluri M, Compagnoni R. 2006. Polyphase inclusions in garnet-orthopyroxenite (Dabie Shan, China) as monitors for metasomatism and fluid-related trace element transfer in subduction zone peridotite. Earth Planet Sci Lett, 249: 173–187

Malaspina N, Hermann J, Scambelluri M. 2009. Fluid/mineral interaction in UHP garnet peridotite. Lithos, 107: 38–52

Mallik A, Dasgupta R. 2012. Reaction between MORB-eclogite derived melts and fertile peridotite and generation of ocean island basalts. Earth Planet Sci Lett, 329–330: 97–108

Mallik A, Dasgupta R. 2013. Reactive infiltration of MORB-eclogite-derived carbonated silicate melt into fertile peridotite at 3 GPa and genesis of alkalic magmas. J Petrol, 54: 2267–2300

Manning C E. 2004. The chemistry of subduction-zone fluids. Earth Planet Sci Lett, 223: 1–16

Martin A M, Laporte D, Koga K T, Kawamoto T, Hammouda T. 2012. Experimental study of the stability of a dolomite+coesite assemblage in contact with peridotite: Implications for sediment-mantle interaction and diamond formation during subduction. J Petrol, 53: 391–417

Massonne H J. 2003. A comparison of the evolution of diamondiferous quartz-rich rocks from the Saxonian Erzgebirge and the Kokchetav Massif: Are so-called diamondiferous gneisses magmatic rocks? Earth Planet Sci Lett, 216: 347–364

Mo X X, Niu Y L, Dong G C, Zhao Z D, Hou Z Q, Zhou S, Ke S. 2008. Contribution of syncollisional felsic magmatism to continental crust growth: A case study of the Paleogene Linzizong volcanic Succession in southern Tibet. Chem Geol, 250: 49–67

Nicholls I A, Ringwood A E. 1973. Effect of water on olivine stability in tholeiites and production of silica-saturated magmas in the island arc environment. J Geol, 81: 285–300

Nomade S, Renne P R, Mo X X, Zhao Z D, Zhou S. 2004. Miocene volcanism in the Lhasa block, Tibet: Spatial trends and geodynamic implications. Earth Planet Sci Lett, 221: 227–243

Patiño Douce A E, Beard J S. 1995. Dehydration-melting of biotite gneiss and quartz amphibolite from 3 to 15 kbar. J Petrol, 36: 707–738

Patiño Douce A E. 2005. Vapor-absent melting of tonalite at 15–32 kbar. J Petrol, 46: 275–290

Perchuk A L, Burchard M, Maresch W V, Schertl H P. 2005. Fluid-mediated modification of garnet interiors under ultrahigh-pressure conditions. Terra Nova, 17: 545–553

Perchuk A L, Burchard M, Maresch W V, Schertl H P. 2008. Melting of hydrous and carbonate mineral inclusions in garnet host during ultrahigh pressure experiments. Russ Geol Geophys, 103: 25–45

Perchuk A L, Shur M Yu, Yapaskurt V O, Podgornova S T. 2013. Experimental modeling of mantle metasomatism coupled with eclogitization of crustal material in a subduction zone. Petrology, 21: 579–598

Perchuk A L, Yapaskurt V O. 2013. Experimental simulation of orthopyroxene enrichment and carbonation in the suprasubduction mantle under the influence of H_2O, CO_2, and SiO_2. Geochem Int, 51: 257–268

Qian Q, Hermann J. 2013. Partial melting of lower crust at 10–15 kbar: Constraints on adakite and TTG formation. Contrib Mineral Petrol, 165: 1195–1224

Qu X M, Hou Z Q, Li Y G. 2004. Melt components derived from a subducted slab in late orogenic ore-bearing porphyries in the Gangdese copper belt, southern Tibetan plateau. Lithos, 74: 131–148

Rapp R P, Watson E B. 1995. Dehydration melting of metabasalt at 8–32 kbar: Implications for continental growth and crust-mantle recycling. J Petrol, 36: 891–931

Rapp R P, Shimizu N, Norman M D, Applegate G S. 1999. Reaction between slab-derived melts and peridotite in the mantle wedge: Experimental constraints at 3.8 GPa. Chem Geol, 160: 335–356

Rapp R P, Norman M D, Laporte D, Yaxley G M, Martin H, Foley S F. 2010. Continent formation in the Archean and chemical evolution of the cratonic lithosphere: Melt-rock reaction experiments at 3–4 GPa and petrogenesis of Archean Mg-diorites (sanukitoids). J Petrol, 51: 1237–1266

Royden L H, Burchfiel B C, van der Hilst R D. 2008. The geological evolution of the Tibetan Plateau. Science, 321: 1054–1058

Rudnick R L, Gao S. 2003. Composition of the continental crust. In: Rudnick R L, ed. Treatise in Geochemistry: The Crust. Amsterdam: Elsevier. 1–64

Russell J K, Porritt L A, Lavallée Y, Dingwell D B. 2012. Kimberlite ascent by assimilation-fuelled buoyancy. Nature, 481: 352–357

Schmidt M W, Poli S. 1998. Experimentally based water budgets for dehydration slabs and consequences for arc magma generation. Earth Planet Sci Lett, 163: 361–379

Sekine T, Wyllie P J. 1982a. Phase relationships in the system $KAlSiO_4$-Mg_2SiO_4-SiO_2-H_2O as a model for hybridization between hydrous siliceous melts and peridotite. Contrib Mineral Petrol, 79: 368–374

Sekine T, Wyllie P J. 1982b. The system granite-peridotite-H_2O at 30 kbar, with applications to hybridization in subduction zone magmatism. Contrib Mineral Petrol, 81: 190–202

Sekine T, Wyllie P J. 1983. Experimental simulation of mantle hybridization in subduction zones. J Geol, 91: 511–528

Sen C, Dunn T. 1994a. Dehydration melting of a basaltic composition amphibolite at 1.5 GPa and 2.0 GPa: Implication for the origin of adakites. Contrib Mineral Petrol, 117: 394–409

Sen C, Dunn T. 1994b. Experimental modal metasomatism of a spinel lherzolite and the production of amphibole-bearing peridotite. Contrib Mineral Petrol, 119: 422–432

Shatsky V S, Jagoutz E, Sobolev N V, Kozmenko O A, Parkhomenko V S, Troesch M. 1999. Geochemistry and age of ultrahigh pressure metamorphic rocks from the Kokchetav massif (Northern Kazakhstan). Contrib Mineral Petrol, 137: 185–205

Shaw C S J, Dingwell D B. 2008. Experimental peridotite-melt reaction at one atmosphere: A textural and chemical study. Contrib Mineral Petrol, 155: 199–214

Shreve R L, Cloos M. 1986. Dynamics of sediment subduction, mélange formation, and prism accretion. J Geophys Res, 91: 10229–10245

Skjerlie K P, Johnston A D. 1996. Vapour-absent melting from 10 to 20 kbar of crustal rocks that contain multiple hydrous phases: Implications for anatexis in the deep to very deep continental crust and active continental margins. J Petrol, 37: 661–691

Skjerlie K P, Patiño Douce A E. 2002. The fluid-absent partial melting of a zoisite-bearing quartz eclogite from 1.0 to 3.2 GPa: Implications for melting in thickened continental crust and for subduction-zone processes. J Petrol, 43: 291–314

Song Y R, Xu H J, Zhang J F, Wang D Y, Liu E D. 2014a. Syn-exhumation partial melting and melt segregation in the Sulu UHP terrane: Evidences from leucosome and pegmatitic vein of migmatite. Lithos, 202–203: 55–75

Song Y R, Xu H J, Zhang J F, Wang D Y, Liu E D. 2014b. Effects of melt fractional crystallization on Sr-Nd and Lu-Hf isotope systems: A case study of Triassic migmatite in the Sulu UHP terrane. Int Geol Rev, 56: 783–800

Spandler C, Pirard C. 2013. Element recycling from subducting slabs to arc crust: A review. Lithos, 170: 208–223

Springer W, Seck H A. 1997. Partial fusion of basic granulite at 5 to 15 kbar: Implications for the origin of TTG magmas. Contrib Mineral Petrol, 127: 30–45

Stöckhert B, Duyster J, Trepmann C, Massonne H J. 2001. Microdiamond daughter crystals precipitated from supercritical COH+silicate fluids included in garnet, Erzgebirge, Germany. Geology, 29: 391–394

Sweeney R J, Prozesky V, Przybylowicz W. 1995. Selected trace and minor element partitioning between peridotite minerals and carbonatite melts at 18–46 kb pressure. Geochim Cosmochim Acta, 59: 3671–3683

Tao R, Fei Y, Zhang L. 2013. Experimental determination of siderite stability at high pressure. Am Mineral, 98: 1565–1572

Tatsumi Y, Eggins S. 1995. Subduction Zone Magmatism. Oxford: Blackwell Science. 211

Wallis S, Tsuboi M, Suzuki K, Fanning M, Jiang L, Tanaka T. 2005. Role of partial melting in the evolution of the Sulu (eastern China) ultrahigh-pressure terrane. Geology, 33: 129–132

Wang C G, Liang Y, Xu W L, Dygert N. 2013. Effect of melt composition on basalt and peridotite interaction: laboratory dissolution experiments with applications to mineral compositional variations in mantle xenoliths form the North China Craton. Contrib Mineral Petrol, 166: 1469–1488

Wang L, Kusky T M, Polat A, Wang S J, Jiang X F, Zong K Q, Wang J P, Deng H, Fu J M. 2014. Partial melting of deeply subducted eclogite from the Sulu orogen in China. Natu Commun, 5: 5604, doi: 10.1038/ncomms6604

Wang Q, Wyman D A, Xu J F, Jian P, Zhao Z H, Li C F, Xu W, Ma J L, He B. 2007. Early Cretaceous adakitic granites in the Northern Dabie Complex, central China: Implications for partial melting and delamination of thickened lower crust. Geochim Cosmochim Acta, 71: 2609–2636

Wang X, Liu J G, Mao H K. 1989. Coesite-bearing eclogite from the Dabie Mountain in central China. Geology, 17: 1085–1088

Wen D R, Liu D Y, Chung S L, Chu M F, Ji J Q, Zhang Q, Song B, Lee T Y, Yeh M W, Lo C H. 2008. Zircon SHRIMP U-Pb ages of the Gangdese Batholith and implications for Neotethyan subduction in southern Tibet. Chem Geol, 252: 191–201

Whitney D L, Teyssier C, Rey P F. 2009. The consequences of crustal melting in continental subduction. Lithosphere, 1: 323–327

Wolf M B, Wyllie P J. 1994. Dehydration-melting of amphibolite at 10 kbar: The effects of temperature and time. Contrib Mineral Petrol, 115: 369–383

Wu Y B, Zheng Y F, Zhao Z F., Gong B, Liu X, Wu F Y. 2006. U-Pb, Hf and O isotope evidence for two episodes of fluid-assisted zircon growth in marble-hosted eclogites from the Dabie orogen. Geochim Cosmochim Acta, 70: 3743–3761

Wyllie P J, Sekine T. 1982. The formation of mantle phlogopite in subduction zone hybridization. Contrib Mineral Petrol, 79: 375–380

Wyllie P J, Carroll M R, Johnston A D, Rutter M J, Sekine T, Van Der Laan S R. 1989. Interactions among magmas and rocks in subduction zone regions: experimental studies from slab to mantle to crust. Eur J Mineral, 1: 165–179

Xia Q X, Zheng Y F, Zhou L G. 2008. Dehydration and melting during continental collision: Constraints from element and isotope geochemistry of low-T/UHP granitic gneiss in the Dabie orogen. Chem Geol, 247: 36–65

Xie Z, Zheng Y F, Zhao Z F, Wu Y B, Wang Z R, Chen J F, Liu X M, Wu F Y. 2006. Mineral isotope evidence for the contemporaneous process of Mesozoic granite emplacement and gneiss metamorphism in the Dabie orogen. Chem Geol, 231: 214–235

Xiong X L, Adam J, Green T H. 2005. Rutile stability and rutile/melt HFSE partitioning during partial melting of hydrous basalt: Implications for TTG genesis. Chem Geol, 218: 339–359

Xu H J, Ma C Q, Ye K. 2007. Early Cretaceous granitoids and their implications for Collapse of the Dabie orogen, eastern China: SHRIMP zircon U-Pb dating and geochemistry. Chem Geol, 240: 238–259

Xu H J, Ma C Q, Zhang J F. 2012a. Generation of Early Cretaceous high-Mg adakitic host and enclaves by magma mixing, Dabie orogen, Eastern China. Lithos, 142–143: 182–200

Xu H J, Ma C Q, Zhang J F, Ye K. 2012b. Early Cretaceous low-Mg adakitic granites from the Dabie orogen, eastern China: Petrogenesis and implications for destruction of the over-thickened lower continental crust. Gondwana Res, 23: 190–207

Xu H J, Ma C Q, Song Y R, Zhang J F, Ye K. 2012c. Early Cretaceous intermediate-mafic dykes in the Dabie orogen, eastern China: Petrogenesis and implications for crust-mantle interaction. Lithos, 154: 83–99

Xu H J, Ye K, Song Y, Chen Y, Zhang J F, Liu Q, Guo S. 2013. Prograde metamorphism, decompressional partial melting and subsequent melt fractional crystallization in the Weihai migmatitic gneisses, Sulu UHP terrane, eastern China. Chem Geol, 341: 16–37

Xu H J, Zhang J F, Wang Y F, Liu W L. 2015. Late Triassic alkaline complex in the Sulu UHP terrane: Implications for post-collisional magmatism and subsequent fractional crystallization. Gondwana Res, doi: 10.1016/j.gr.2015.05.017

Xu W C, Zhang H F, Guo L, Yuan H L. 2009. Miocene high Sr/Y magmatism, south Tibet: Product of partial melting of subducted Indian continental crust and its tectonic implication. Lithos, 114: 293–306

Xu W L, Zhou Q J, Pei F P, Yang D B, Gao S, Li Q L, Yang Y H. 2013. Destruction of the North China Craton: delamination or thermal/Chemical erosion? Mineral chemistry and oxygen isotope insights from websterite xenoliths. Gondwana Res, 23: 119–129

Xu S T, Okay A I, Ji S, Sengor A M C, Su W, Liu Y, Jiang L. 1992. Diamond from the Dabie Shan meta-morphic rocks and its implication for tectonic setting. Science, 256: 80–82

Yang J H, Chung S L, Wilde S A, Wu F Y, Chu M F, Lo C H, Fan H R. 2005. Petrogenesis of post-orogenic syenites in the Sulu Orogenic Belt, East China: Geochronological, geochemical and Nd-Sr isotopic evidence. Chem Geol, 214: 99–125

Yang Q L, Zhao Z F, Zheng Y F. 2012a. Modification of subcontinental lithospheric mantle above continental subduction zone: Constraints from geochemistry of Mesozoic gabbroic rocks in southeastern North China. Lithos, 146–147: 164–182

Yang Q L, Zhao Z F, Zheng Y F. 2012b. Slab-mantle interaction in continental subduction channel: Geochemical evidence from Mesozoic gabbroic intrusives in southeastern North China. Lithos, 155: 442–460

Yang D B, Xu W L, Pei F P, Yang C H, Wang Q H. 2012. Spatial extent of the influence of the deeply subducted Yangtze slab on the eastern North China Craton lithosphere: Constraints from Sr-Nd-Pb isotopic compositions of Mesozoic mafic igneous rocks in western Shandong, China. Lithos, 136–139: 246–260

Yaxley G M. 2000. Experimental study of the phase and melting relations of homogeneous basalt plus peridotite mixtures and implications for the petrogenesis of flood basalts. Contrib Mineral Petrol, 139, 326–338

Yaxley G M, Brey G P. 2004. Phase relations of carbonate-bearing eclogite assemblages from 2.5 to 5.5 GPa: Implications for petrogenesis of carbonatites. Contrib Mineral Petrol, 146: 606–619

Ye K, Cong B L, Ye D N. 2000. The possible subduction of continental material to depths greater than 200 km. Nature, 407: 734–736

Zhang J F, Wang C, Wang Y F. 2012. Experimental constraints on the destruction mechanism of the North China Craton. Lithos, 149: 91–99

Zhang J, Zhao Z F, Zheng Y F, Liu X M, Xie L W. 2012. Zircon Hf-O isotope and whole-rock geochemical constraints on origin of postcollisional mafic to felsic dykes in the Sulu orogen. Lithos, 136–139: 225–245

Zhang R Y, Yang J S, Wooden J L, Liou J G, Li T F. 2005. U-Pb SHRIMP geochronology of zircon in garnet peridotite from the Sulu UHP terrane, China: Implication for mantle metasomatism and subduction-zone UHP metamorphism. Earth Planet Sci Lett, 237: 729–734

Zhang Z M, Dong X, Liou J G, Liu F, Wang W, Yui F. 2011. Metasomatism of garnet peridotite from Jiangzhuang, southern Sulu UHP belt: Constraints on the interactions between crust and mantle rocks during subduction of continental lithosphere. J Metamorph Geol, 29: 917–937

Zhao Z D, Mo X X, Dilek Y, Niu Y, DePaolo D J, Robinson P, Zhu D, Sun C, Dong G, Zhou S, Luo Z, Hou Z. 2009. Geochemical and Sr-Nd-Pb-O isotopic compositions of the post-collisional ultrapotassic magmatism in SW Tibet: Petrogenesis and implications for India intra-continental subduction beneath southern Tibet. Lithos, 113: 190–212

Zhao Z F, Zheng Y F, Chen R X, Xia Q X, Wu Y B. 2007. Element mobility in mafic and felsic ultrahigh-pressure metamorphic rocks during continental collision. Geochim Cosmochim Acta, 71: 5244–5266

Zhao Z F, Zheng Y F, Wei C S, Wu F Y. 2011. Origin of postcollisional magmatic rocks in the Dabie orogen: Implications for crust-mantle interaction and crustal architecture. Lithos, 126: 99–114

Zhao Z F, Zheng Y F, Zhang J, Dai L Q, Li Q, Liu X. 2012. Syn-exhumation magmatism during continental collision: Evidence from alkaline intrusives of Triassic age in the Sulu orogen. Chem Geol, 328: 70–88

Zhao Z F, Dai L Q, Zheng Y F. 2013. Postcollisional mafic ignieous rocks record crust-mantle interaction during continental deep subduction. Scientific Reports, 3: 3413, doi: 10.1038/srep03413

Zheng Y F. 2009. Fluid regime in continental subduction zones: Petrological insights from ultrahigh-pressure metamorphic rocks. J Geol Soc Lond, 166: 763–782

Zheng Y F, Xia Q X, Chen, R X, Gao X Y. 2011. Partial melting, fluid supercriticality and element mobility in ultrahigh-pressure metamorphic rocks during continental collision. Earth-Sci Rev, 107: 342–374

Zheng Y F. 2012. Metamorphic chemical geodynamics in continental subduction zones. Chem Geol, 328: 5–48

Zheng Y F, Hermann J. 2014. Geochemistry of continental subduction-zone fluids. Earth Planets Space, 66: 93, doi: 10. 1186/1880-5981-66-93

Zhou L G, Xia Q X, Zheng Y F, Chen R X, Hu Z C, Yang Y H. 2015. Tectonic evolution from oceanic subduction to continental collision during the closure of Paleotethyan ocean: Geochronological and geochemical constraints from metamorphic rocks in the Hong'an orogen. Gondwana Res, 28: 348–370

Zindler A, Hart S. 1986. Chemical geodynamics. Annu Rev Earth Planet Sci, 14: 493–571

Zong K Q, Liu Y S, Hu Z C, et al. 2010. Melting-induced fluid flow during exhumation of gneisses of the Sulu ultrahigh-pressure terrane. Lithos, 120: 490–510